Full Paper

FINITE ELEMENT MODELING OF AN ALUMINUM ALLOY AUTOMOBILE RIM UNDER STATIC LOAD

D.A. Fadare
Department of Mechanical Engineering, University of Ibadan, P.M.B 1, Ibadan, Nigeria
fadareda@yahoo.com

O.O. Odebunmi
Department of Mechanical Engineering, University of Ibadan, P.M.B 1, Ibadan, Nigeria

S..O. Igbudu
Department of Mechanical Engineering, Ambrose Alli University, Ekpoma, Nigeria

ABSTRACT

Rims are essential safety components for support, steering, mobility and break systems in automobile. Aluminum alloy rims are commonly used in the automobile industry due to their durability, light weight, high strength, good heat conductor, wear resistance and aesthetics characteristics. However, their structural integrity under diverse operating conditions is not well understood. In this study, the combined effects of static loads due to varying automobile weights and tyre air inflation pressures on the total displacement, von Mises stress and principal strain of an aluminum alloy automobile rim (Toyota 6.0JX15H2ET, CMS190CN604) was investigated using a commercially available 3-dimensional finite element code in FEMLAB® 3.0. The effects of the loading condition were investigated at the point of contact of tyre with the ground; outboard and inboard bead seats; and the well. Results showed that maximum deflection occurred at the inboard bead seat, while the most stressed area occurred at the well. Increase in automobile weight and tyre inflation pressure led to increased state of stress and strain. This study provides basic insights into the state of stress in aluminum alloy rims under diverse loading conditions.

Keywords: *Finite element method, aluminum alloy rim, automobile, structural analysis, von Mises stress, principal strain*

1. INTRODUCTION

Rims are essential safety components for support, steering, mobility and breaking systems in automobile. There are important structural members of the vehicular suspension system that supports the static and dynamic loads encountered during vehicle operation (Cerit, 2010). Automobile rims have evolved over the decades from early spoke designs of wood and steel rims, carryovers from wagon and bicycle technology, to flat steel discs and finally to the stamped metal configurations and modern cast and forged aluminum alloy rims of today's modern vehicles (Stearns, 2000). The main features and nomenclature of modern automobile rims are shown in a ¼ section of the rim in Figure 1

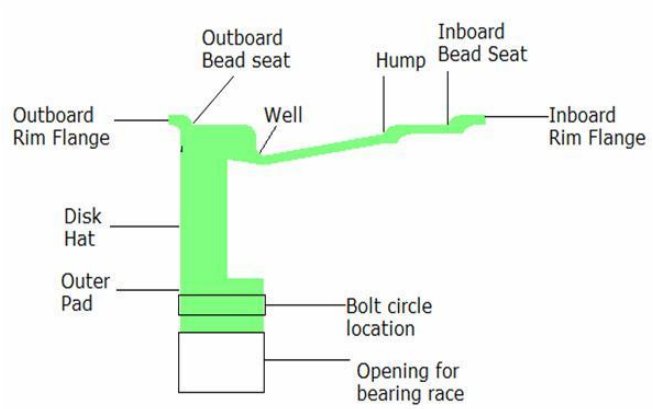

Figure 1: Automobile rim (Stearns, 2000)

The global concern for reduction in greenhouse gas emissions and the associated climate change of the Kyoto protocol (IPCC, 1995) is a major compelling factor driving the automobile industry in their efforts to reduce weight of vehicle in order to improve the fuel efficiency. Hence, light aluminum alloys are currently enjoying wider applications in the automobile industry (Stearns, 2000). In particular, aluminum alloy rims are becoming increasingly popular in automobile rim manufacture on account of numerous advantages over the wooden and steel rims which include: durability, light weight, high strength, good heat conductor, wear resistance and aesthetics attributes (Stearns, 2000). Automobile rims are loaded in complex manner and are highly stressed and therefore safety related components. Hence, fatigue performance and the state of stress in the rim under various loading conditions are prime concerns in vehicle design (Stearns, 2000; Cerit, 2010). Historically, successful designs are achieved after years of experience and extensive field testing. Several innovative methods of testing and experimental stress measurements have been developed (Kruse and Mahnig, 1976). In recent years, the procedures have been improved by a variety of experimental and analytical methods for structural analysis (Stearns, 2000). The earliest published reports span the mid 1970s and most dealt primarily with impact strength and dynamic testing of steel and aluminum alloy wheels (Stearns, 2000). These analytical methods are known to be complex and strong theoretical backgrounds are required, while the experimental methods are costly and time consuming. To this effect, application of numerical methods such as finite element method (FEM) is currently gaining

more ground in structural analysis of automobile rims (Stearns, 2000). Rihda (1976) applied the finite element method to determine the total required strength, and optimum distribution of stress and strain in automobile wheels. Morita *et al.* (1987; 1989), Tanaka *et al.* (1987), Wright (1983) and Kawashima and Ishihara (1989) used the finite element method to simulate the dynamic effects of rolling, cornering and braking loads in steel rims. Reipert (1985) and Mizoguchi *et al.* (1982) performed a series of finite element analysis on aluminum alloy 5454 rim using NASTRAN to rationalize the fatigue design. Morita *et al.* (1987) performed a 3-dimensional finite element stress evaluation for wheels during endurance tests. Kawashima and Ishihara (1989) developed a quantitative method for evaluating the induced stress of the automobile rim. Konishi *et al.* (1996; 1997) attempted parametric studies on impact strength in aluminum wheels where typical aluminum alloy wheels of various dimensions were analyzed. It was found that impact strength was characterized by rim flange thickness and spoke rigidity when the rim flange failure occurred.

Studies on the influence of varying radial loading due to vehicle weight, tyre inflation pressure, braking and cornering load conditions on the fatigue life of the rims have been the focus of many researchers in order to ascertain the structural stability and hence the safety of automobile rims during their working life span. Tseng (1989) and Jeusette (1992) investigated the tyre rim interface under radial loading conditions. Jeusette (1992) studied the effect of inflation pressure variations on the tyre/rim interface loading and concluded that reducing inflation pressure by half reduced the imposed stress in same magnitude. Walter and Kiminecz (1975) have reported a finite element analysis of the effect of heavy braking and cornering maneuvers on the contact pressure and shear stress distributions of automobile tyre/rim interface. Cerit (2010) has reported an experimental and numerical simulation of dynamic impact loading of a cast aluminum alloy wheel due to collision with the curb of the road or a large obstacle. The result obtained showed that the maximum stress occurred in the lug region of the wheel. This was primarily attributed to the fact that the lug hole forms geometrical complexities and irregularities in this region.

Stearns (2000) and Stearns *et al.* (2004) reported an experimental and finite element study on the analysis of displacement, stress and strain distributions in an automobile wheel consisting of an aluminum alloy rim (Ford 16`` SHO style) and a run-flat tyre (P22560R16). The study evaluated the conjoint influence of static load due to tyre inflation and radial loads due to the vehicle weight on the displacement, stress and strain fields. Apart from the works of Stearns (2000) and Stearns *et al.* (2004), limited studies have been reported on the finite element analysis of structural characteristics (displacement, stress and strain distributions) of aluminum alloy rim designs. New designs of these rims are being developed on continuous basis and the determination of structural performance of these wheels is essential for their safe operations, but the physical testing and inspection of the wheels during their development process is time consuming and costly. Therefore, it is important to reduce the time spent during the development and testing phase of new rims by using numerical simulation methods such as finite element analysis. The aim of this present study was to develop a 3-dimensional finite element model for the analysis of the combined effects of static load due to varying automobile weights and tyre air inflation pressures on the total displacement, von Mises stress and principal strain distributions in a new generation, aluminum alloy automobile rim (Toyota 6.0JX15H2ET, CMS190CN604).

2. Materials And Methods

A new generation, aluminum alloy automobile rim (Toyota 6.0JX15H2ET, CMS190CN604) of 15" (0.381 m) diameter, 7.48" (0.190 m) width, 2.68" (0.068 m) hub opening diameter and 0.74" (0.0188 m) bolt circle diameter, bead seat radius of 15.9" (0.2021 m) and bead seat width of 0.98" (0.025 m) was modeled using commercial FEMLAB 3.0 code The rim-tyre assembly and the finite element model are shown in Figures 2 (a & b). A total of 478,672 iso-parametric elements with 1,839,630 degree-of-freedom were used in the model. The mechanical and chemical properties of the aluminum alloy 3003-H18 rim are summarized in Tables 1 and 2, respectively.

Table 1: Mechanical properties of the aluminum alloy 3003-H18 rim

Property	Value
Young's modulus (Pa)	$69e^{9}$
Poisson's ratio	0.33
Density (kg/m^3)	2730
Thermal expansion coeff.	$23.2e^{-6}$
Heat capacity (J/K)	893
Thermal conductivity (W/m*K)	155

Source: FEMLAB (2004)

2.1. Modeling the effect of automobile weight on the rim

The eye-bar loading technique (Stearns, 2000) was used to model the effect of the vehicle weight on the rim. The technique is illustrated diagrammatically in Figure 3.

Table 2: Chemical properties of the aluminum alloy 3003-H18 rim

Element	Value
Aluminum	Balance
Copper	0.05 - 0.2
Iron	0.7 max
Manganese	1 - 1.5
Remainder Each	0.05 max
Remainder Total	0.15 max
Silicon	0.6 max
Zinc	0.1 max

Source: Material Property Data Sheet (2011)

(a)

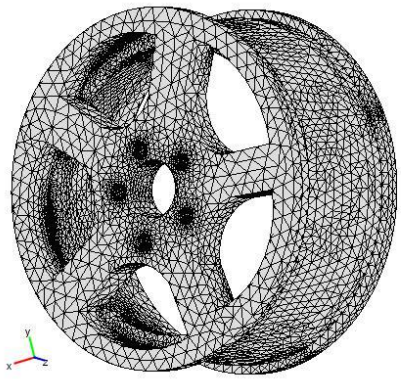

(b)

Fig 2: The rim-tyre assembly (a) and finite element model (b) of the aluminum alloy rim

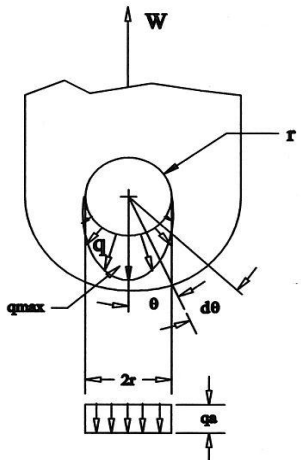

Fig 3: Schematic diagram of eye-bar analogy (Stearns, 2000)

Where, r is the radius of the hole, W is the load imparted, θ is the angle and qmax is the maximum point load. The horizontal components of q are in balance with each other. The vertical forces can be related to the external load, W which is expressed as follows (Stearns, 2000):

$$W = 2 * r \int_0^{\pi/2} q * \cos\theta d\theta \quad (1)$$

By defining $q = q_{\max} * \cos\theta$ and substituting into the above equation (Stearns, 2000),

$$W = 2 * r \int_0^{\pi/2} q_{\max} * \cos^2\theta d\theta \quad (2)$$

integrating yields (Stearns, 2000)

$$W = 2 * r * q_{\max} * \left[\frac{\theta}{2} + \frac{(\sin 2\theta)}{4}\right]_0^{\pi/2} \quad (3)$$

Evaluating (Stearns, 2000),

$$W = 2 * r * q_{\max} * \left[\left(\frac{\pi/2}{2} + \frac{\sin 2 * \pi/2}{4}\right) - (0)\right] \quad (4)$$

or

$$q_{\max} = \frac{2 * W}{\pi * r} \quad (5)$$

$q_{\max}$ is in unit load and r is the radius of the bead seat (0.2021 m). Normally this radius is assumed to be nearly equal to the pin radius. Dividing $q_{\max}$ by its width of the eye-bar cross section gives the compressive pressure load.

$$\text{Pressure load} = q_{\max} / b \quad (6)$$

Where b is the width of the bead seat (0.025 m). The total weight of a car is balanced with a vertical reaction force from the road through the tyre. This load constantly compresses the wheel radially. While the car is running, the radial load becomes a cyclic load with the rotation of the wheel. Hence, the evaluation of wheel fatigue strength under radial load is an important performance characteristic for structural integrity. According to the SAE specification, a wheel should maintain structural integrity without any cracks or plastic deformation for more than 4 x 10^9 rotations under a radial load. The radial load, Q, is expressed by (Stearns, 2000):

$$Q = S_r * W \quad (7)$$

where, S_r means acceleration test factor $(S_r = 2.2)$ and W means maximum tyre load. Under a radial load, the strength of the rim usually determines the fatigue life of a wheel, so the stress evaluation is mainly focused on the radial load. The radial load is applied from the tyre to the rim through the bead seat therefore the distributed pressure is applied directly on the bead seat. On the assumption that the load is equally or evenly distributed on the four wheels, the weight of the automobile is related to the tyre load, W_t (Stearns, 2000) as:

$$W_t = W_a * 9.8/4 \quad (8)$$

Where W_t is the maximum wheel load and W_a is the maximum mass of the automobile,

2.2. Modeling the tyre inflation pressure on the rim

During the rolling operation of the rim, the cyclically varying stress due to the bending moment or the radial load is superimposed on the constant stress generated by the tyre-air pressure. From structural point of view, it is necessary to precisely evaluate the stress induced by the tyre-air pressure. The tyre air pressure is applied directly to the bead seat and indirectly to the rim flange. The later load, which is directed in an axial direction, is generated by the air pressure pressing on the tyre side wall. This load varies according to the type of tyre, the aspect ratio of the cross section of the tyre and the reinforcement structure of the tyre. The axial component of the force W_p which results from the inflation of the tyre is calculated by the equation (Stearns, 2000):

$$W_p = \pi\left(a^2 - r_f^2\right) P_0 \quad (11)$$

Where a, is the design radius of the tyre, r_f is the radius of the loading point on the rim flange and P_0 is the tyre inflation pressure. Because the axial load is supported by the tread of the tyre and the rim flange, approximately, half of the load is assumed to be loaded on each part. Hence, the load on the circumferential unit length of the rim flange is calculated by the force, T_f, expressed as (Stearns, 2000):

$$T_f = \frac{W_p}{2*2*\pi*r_f} = \left(a^2 - r_f^2\right)*\frac{P_0}{4*r_f} \quad (12)$$

The combined effects of the varying automobile weights (radial loads) of 4630.5, 5218.5 and 5885.5 N and tyre inflation pressures of 117, 241 and 303 kPa on the displacement, von Mises stress and principal strain distributions were investigated. The weight of 4630.5 N represents the normal weight of a 5-seater salon car and five (5) passengers, the 5318.5 N weight represents the weight of the car plus 5 passengers and one (1) extra passenger, while the 5885.5 N represents the weight of the car plus 5 passengers and two (2) extra passengers. The tyre inflation pressure of 241 kPa represents normal tyre inflation pressure, while 117 and 303 kPa represents under and over inflation pressures, respectively. The weights and tyre inflation pressures were combined into three loading conditions: (1) 4630.5 N and 117 kPa; (2) 5218.5 N and 241 kPa; and (3) 5885.5 N and 303 kPa. The effects of the loading conditions were investigated at the point of contact of tyre with the ground; outboard and inboard bead seats; and the well.

2.3. Imposed boundary conditions

To avoid rigid body motion and ensure convergence in the solution, the nodal points of the elements at the circumference of the holes of centre bolts were constrained from translational motion in the three perpendicular directions (x, y, z).

3. Results And Discussion

The influence of the loading condition on the total displacement, von Mises stress and principal strain fields were assessed using the postprocessing and visualization module of the FEMLAB software. The surface plot of the cross-section of the rim model was switched to the different fields showing the total displacement, von Mises stress and principal strain at different points of interest on the rim. The deformed solid model of the rim under the loading condition 3 is shown in Figure 4. The colour map shows total displacement field of the rim.

3.1. Observations at the point of contact with the ground

The influence of the loading condition on the total displacement, von Mises stress and principal strain fields at the point of contact with the ground (0/360° circumferential angle) along the rim width are shown in Figures 5 (a - c). As shown in Figure 5(a), the maximum total displacement in the rim occurred at the inboard bead seat, while no appreciable displacement was observed at the disk hat.

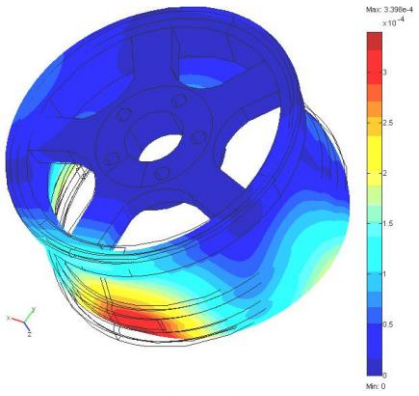

Fig. 4: Deformed rim model under the loading condition 3

Increase in the radial load and tyre inflation pressure as depicted in the loading conditions 1 to 3 led to linear increase in the total displacement. Excessive displacement of the inboard bead seat can lead to sudden dislodgement of the tyre from the rim and thus leading to deflation of tyre which may results to fatal accidents. The von Mises stress distribution for the three loading conditions are shown in Figure 5(b). As shown, the minimum stress occurred at the outboard bead seat and increased to the peak at the rim well for all the loading conditions. For the loading condition 3, the stresses remained constant towards the inboard bead seat, while it decreased for the loading conditions 1 and 2. There was no notable influence of loading condition from the disk hat to the rim well, but notable variation was obtained beyond the rim well to inboard bead seat. The influence of loading condition on the principal strain distributions are shown in Figure 5(c). A similar pattern like stress field was also observed in the strain field. The minimum and maximum strains occurred at the inboard bead seat and the well, respectively. The trends obtained in the total displacement, von Mises stress and principal strain matched perfectly the observations reported by Stearns (Stearns, 2000).

3.2. Observations at the outboard bead seat

Figures 6 (a - c) show the influence of the loading condition on the total displacement, von Mises stress and principal strain fields at the outboard bead seat. As shown in Figure 6(a), the total displacement varied widely along the circumferential angle. Noticeable peaks in the total displacement occurred at 50° and 250o^0 circumferential angles for all the loading conditions. The highest total displacement was obtained for the loading condition 3, while the minimum total displacement occurred at 200o^0 for all the loading conditions. The influence of loading conditions was predominant on the total displacement only between 0 and 100°. The von Mises stress distributions for the three loading conditions are shown in Figure 6(b). It can be seen, that the stresses varied widely along the circumferential angle. Noticeable peaks similar to the displacement field were also obtained at 50° for loading condition 3 and at 250°, for loading conditions 1 and 3. The loading condition 3 had the highest stress magnitude from 0 to 230°, beyond this point, a reverse in the trend was observed. Figure 6(c) shows the influence of loading condition on the principal strain. The strain also varied widely, with maximum strain at 250° for the loading conditions 1 and 2, while for the loading condition 1 the maximum occurred at 50°. Similar to the stress field, the loading condition 3 also had the highest stain magnitude from 0 to 230°, beyond this point, a reverse in the trend was observed. Similar trends have been reported by Stearns (Stearns, 2000).

3.3. Observations at the inboard bead seat

Figures 7 (a - c) depict the influence of the loading condition on the total displacement, von Mises stress and principal strain at the inboard bead seat. The total displacement field is shown in Figure 7(a). The total displacement for all the loading conditions had the maximum value at the point of contact with the ground (0/360° circumferential angle), while the minimum occurred at within 150 to 200° for the loading condition 1 and at 200° for both loading conditions 2 and 3. The displacement was consistently higher with increasing loading condition, except at the point of minimum displacement (200°) where there was no notable effect of loading condition. The von Mises stress distribution is shown in Figure 7(b). The von Mises stress plot for all the loading conditions had the maximum value at the point of contact with the ground (0/360° circumferential angle). The stresses increased with increase in loading condition, except at 80°, where there was no appreciable variation with the loading condition. As shown in Figure 7(c), the

principal strain distribution also varied with increase in loading condition. For each loading condition, the maximum principal strain occurred at the point of contact with the ground (0/360° circumferential angle). The observations of Stearns (2000) were similar to the trends obtained.

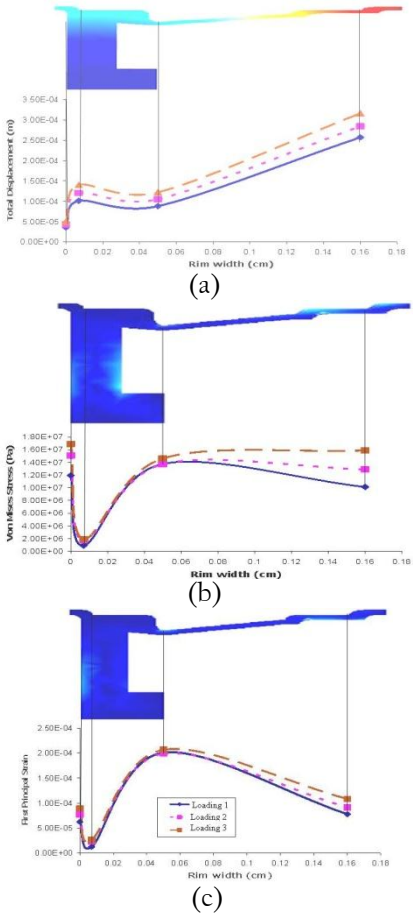

Fig. 5: Influence of loading condition on the total displacement (a), von Mises stress (b) and principal strain (c) distributions at the point of contact with the ground

3.4. Observations at the well

The effect of loading condition on the total displacement, von Mises stress and principal strain at the well are depicted in Figures 8 (a-c). As shown in Figure 8(a), the maximum total displacement occurred at the point of contact (0/360° circumferential angle). The total displacement increased with increase in the loading condition. The minimum values occurred at 100° for the loading condition 1, while for the loading conditions 2 and 3, the minimum occurred at 150o^0. For von Mises stress distribution shown in Figure 8(b), the maximum stress occurred at the point of contact of tyre with the ground (0/360°), while the maximum values for the loading conditions 2 and 3 occurred at angle 90°. The minimum values for the three loading conditions occurred at angle 144°.

The effect of the load condition on the principal strain is shown in Figure 8(c), maximum strain occurred at the point of contact 0/360° and the minimum at angle 90° for the loading

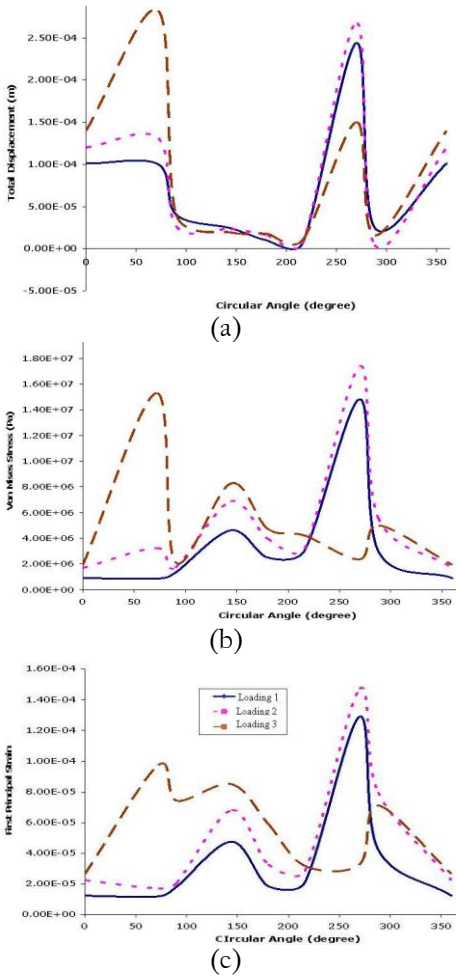

Fig. 6: Influence of loading condition on the total displace (a), von Mises stress (b) and principal strain (c) fields at the outboard bead seat

condition 1 and at 150° for the loading conditions 2 and 3. At angle 270°, a rise in the strain less than the maximum was obtained for loading conditions 2 and 3. These observations were in agreement with the report of Stearns (2000).

4. Conclusion

The combined effects of varying automobile weights and tyre inflation pressures on the total displacement, von Mises stress and principal strain of an aluminum alloy automobile rim has been investigated and the state of stress at the point of contact of tyre with the ground, outboard and inboard bead seats, and the well were presented. For all the loading conditions, maximum deflection occurred at the inboard bead seat, while the most stressed area occurred at the well. Increase in automobile weight and tyre inflation pressure led to increase in state of stress and strain.

References

Cerit, M., "Numerical simulation of dynamic side impact test for an aluminum alloy wheel", Scientific Research and Essays, 5(18):2694-2701, 2010.

FEMLAB "Multiphysics modeling software, version 3.0, user's manual", CONSOL, 2004.

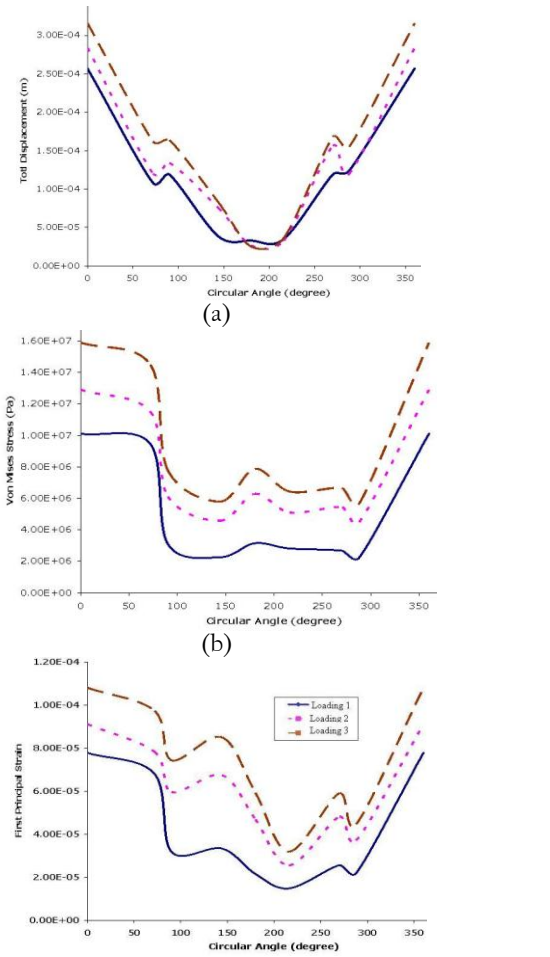

Fig. 7: Influence of loading condition on the total displacement (a), von Mises stress (b) and principal strain (c) fields at the inboard bead seat

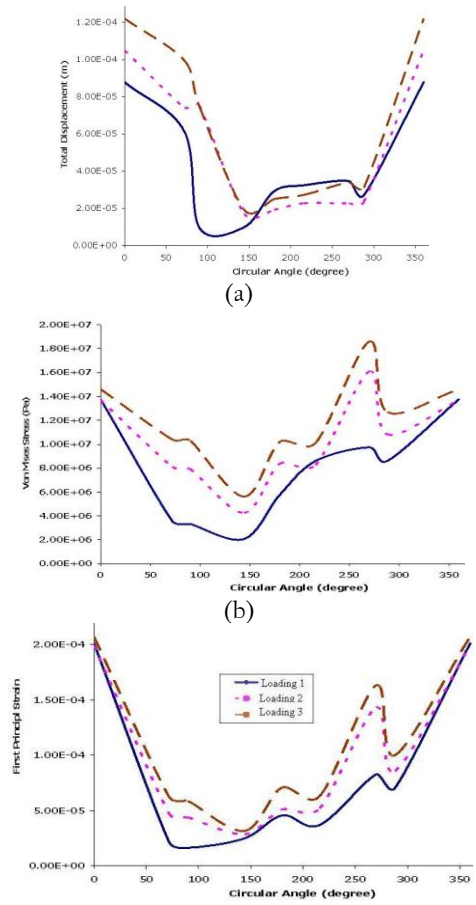

Fig. 8: Influence of loading condition on the total displacement (a), von Mises stress (b) and principal strain (c) fields at the rim well

IPCC (Intergovernmental Panel on Climate Change) "Guidelines for national greenhouse gas inventories, green house gas inventory manual". vol. 3, 1995

Jeusette, T., "Finite element analysis of tire/rim interface forces under braking", Tire Science and Technology, 20(2):83-105, 1992.

Kawashima, H. and Ishihara, K., "Stress evaluation of automotive steel road wheel under radial load", Nippon Kikai Gakkai Ronbunshu, C Hen, 55(513):1254-1258, 1989.

Konishi, H., Fujiwara, A., Katsura, T., Takeuchi, K. and Nakata, M., "Impact strength of Aluminum alloy wheel (Influence of disk and rim rigidity on the JWL impact strength of aluminum alloy wheel", Nippon Kikai Gakkai Ronbunshu, C Hen, 62(599):2884-2890, 1996.

Konishi, H., Fujiwara, A., Katsura, T., Takeuchi, K. and Nakata, M., "Impact strength of aluminum alloy disk wheel", Nippon Kikai Gakkai Ronbunshu, R&D, (Kobe Steel, Ltd), 47(2):25-28, 1997.

Kruse, G. and Mahnig, F., "A comprehensive methods for wheel testing by stress analysis", SAE Technical Paper Series #760042, 1976.

Material Property Data Sheet: *3003 Aluminum* www.suppliersonline.com/*propertypages/3003.asp Retrived, August 2011.*

Mizoguchi, T., Nishimura, H., Nakata, K. and Kawakami, J., "Stress analysis and fatigue strength evaluation of sheet fabricated 2-piece Aluminum alloy wheels for passenger cars", R&D, Research & Development (Kobe Steel, Ltd), 32(2):25-28, 1982.

Morita Y., Kawashima, H. and Ishihara, K., "Induced stress evaluation of automotive steel road wheel during endurance tests", Sumitomo Metals, 41(2):27-34, 1989.

Morita, Y., Kawashima, H., Ishihara, K. and Komatsu, H., "Finite element analysis of a car wheel", Sumitomo Metals, 39(3):245-263, 1987.

Reipert, P., "Optimization of an extremely light cast aluminum alloy wheel rim", International Journal of Vehicle Design, 6(4-5):509-513, 1985.

Rihda, R., "Finite element analysis of automotive wheels", SAE Technical Publication #760085, 1976.

Stearns, J., Srivatsan, T.S. Prakash, A. and Lam P.C., "Modeling the mechanical response of an aluminum alloy automotive rim", Materials Science and Engineering A366 262–268, 2004.

Stearns, J., "An investigation of stress and displacement distribution in a aluminum alloy automobile rim", Dissertation, University of Acorn, USA, 2000.

Tanaka, K., Ishihara, K. and Komatsu, H., "Fatigue strength of car road", 17(2):310-325, 1987.

Tseng, N., "Finite element simulation of the tire rim interface", Tire Science and Technology, 17(2):310-325, 1989.

Walter, J. and Kiminecz, R., "Bead contact pressure measurements at the tire rim interface", SAE technical publication #750458, 1975

Wright, D., "Test methods for automotive wheels", I. Mech. E. Publications, Conference Code 03757, 1983.